Algal Research 91 (2025) 104271

Contents lists available at ScienceDirect

Algal Research

journal homepage: www.elsevier.com/locate/algal

Exploring activated carbon-based microalgae residue to improve CO_2 adsorption performance

Low Yi Chian [a], Umi Fazara Md Ali [a,b,*], Farihahusnah Hussin [c], Mohamed Kheireddine Aroua [c,d], Naimah Ibrahim [e], Mohd Azmier Ahmad [f]

[a] Faculty of Chemical Engineering & Technology, Universiti Malaysia Perlis, Kompleks Pusat Pengajian Jejawi, 02600 Arau, Perlis, Malaysia
[b] Centre of Excellence for Biomass Utilization (COEBU), Universiti Malaysia Perlis, 02600 Arau, Perlis, Malaysia
[c] Research Centre for Carbon Dioxide Capture and Utilization (CCDCU), Faculty of Engineering and Technology, Sunway University, No. 5 Jalan Universiti, Bandar Sunway, 47500 Petaling Jaya, Selangor, Malaysia
[d] School of Engineering, Lancaster University, Lancaster LA1 4YW, United Kingdom
[e] Faculty of Civil Engineering & Technology, Universiti Malaysia Perlis, Kompleks Pusat Pengajian Jejawi, 02600 Arau, Perlis, Malaysia
[f] School of Chemical Engineering, Engineering Campus, Universiti Sains Malaysia, 14300 Nibong Tebal, Penang, Malaysia

ARTICLE INFO

Keywords:
CCUS
Activated carbon
Microalgae residue
Carbon dioxide
Adsorption

ABSTRACT

The rising atmospheric carbon dioxide (CO_2) levels have driven interest in Carbon Capture and Storage (CCS) technologies. Adsorption technology has gained significant attention because of its cost-effectiveness, high efficiency, and scalability. This study focused on producing activated carbon from *Nannochloropsis gaditana* microalgal residue (post-lipid extraction) using a one-step KOH activation and carbonization method. The resulting activated carbon was characterized using scanning electron microscopy combined with energy-dispersive X-ray spectroscopy (SEM-EDX) to examine the surface morphology, Brunauer-Emmett-Teller (BET) analysis to determine the surface area and porosity, and Fourier Transform Infrared Spectroscopy (FTIR) to identify the surface functional groups. CO_2 adsorption performance was evaluated at different temperatures (25, 40, and 55 °C) and inlet feed flow rates (200 and 400 mL/min). The kinetics of CO_2 adsorption and regeneration of activated carbon were examined. SEM results showed successful activation of the microalgae-residue with mesopores and micropores, while EDX showed an increase in carbon content in the activated carbon compared to raw microalgae residue. BET result showed that the prepared activated carbon has a surface area of 296.96 m2/g, average pore diameter of 2.26 nm and total pore volume of 0.17 cm3/g. The presence of oxygen-containing surface functional groups such as hydroxyl (OH) and carbonyl (C=O) in activated carbon were confirmed by FTIR spectroscopy. The highest adsorption capacity of 0.55 mmol/g was obtained at 25 °C and 400 mL/min. The longest breakthrough time (7 min) was observed at 25 °C and 200 mL/min. In this study, CO_2 adsorption followed pseudo-first-order kinetics, and a regeneration study showed good stability of activated carbon over four cycles.

1. Introduction

In recent years, increasing awareness of climate change and its associated impacts has driven global efforts toward reduce greenhouse gas emissions (GHG). GHGs include carbon dioxide (CO_2), methane (CH_4), nitrous oxide (N_2O), hydrofluorocarbons (HFCs), perfluorocarbon (PFCs), sulfur hexafluoride (SF_6,) and nitrogen trifluoride (NF_3) [1]. Each GHG varies in its sources, impact, and atmospheric lifespans, which is quantified as Global Warming Potential (GWP). CO_2 is the predominant GHG emitted from the combustion of fossil fuels in power generation, transportation, and industrial processes. Despite having the lowest GWP of 1, CO_2 remains the leading contributor to climate change because it accounts for approximately 64 % of the global warming effect due to fossil fuel combustion and cement production [2]. CO_2 levels have significantly increased from 340 ppm in 1980 to 415 ppm by 2020 and are projected to reach 570 ppm by 2100 [3,4].

To address these impacts, international efforts such as the Paris Agreement aim to limit global temperature rise to below 2 °C, and

* Corresponding author at: Faculty of Chemical Engineering & Technology, Universiti Malaysia Perlis, Kompleks Pusat Pengajian Jejawi, 02600 Arau, Perlis, Malaysia.
E-mail address: umifazara@unimap.edu.my (U.F.M. Ali).

https://doi.org/10.1016/j.algal.2025.104271
Received 5 June 2025; Received in revised form 29 July 2025; Accepted 18 August 2025
Available online 22 August 2025

ideally 1.5 °C, compared to pre-industrial levels [5]. Malaysia, for instance, has pledged to reduce the carbon intensity of its Gross Domestic Product (GDP) by 45 % by 2030 compared to the 2005 levels [5]. In line with this, Malaysia introduced the National Sustainability Reporting Framework (NSRF) to mandate the reporting of GHG emissions and sustainability statements from listed companies and those with a large market capital of at least RM2 billion [6]. This initiative aims to support nationwide emission reduction goals. There are three main approaches for lowering total CO_2 emissions in the atmosphere: reducing energy intensity, lowering carbon intensity, and increasing CO_2 sequestration. The first approach focuses on improving energy efficiency, while the second involves transitioning to non-fossil fuel sources such as hydrogen and renewable energy. The third approach focuses on advancing technologies to capture and store more CO_2 [7]. Recent research has shifted its focus to developing technologies for CO_2 capture and sequestration, aiming to curtail atmospheric CO_2 levels and mitigate climate-related risks. Among these technologies, adsorption-based systems have emerged as a promising approach because of their efficiency, cost-effectiveness, and relative simplicity of operation compared to other methods such as cryogenic distillation and membrane separation [8]. Although membrane separation is continuous and easy to operate, its effectiveness is limited at low CO_2 concentrations [9].

Activated carbon (AC) is widely used as an adsorbent in CO_2 capture systems owing to its high surface area, porous structure, and favorable chemical properties. It can be produced from any carbon-rich material but traditional sources of activated carbon such as coal are non-renewable and environmentally unsustainable [10]. Biomass feedstock has been extensively explored as a sustainable alternative. These include straw, wood, olive husk, fruit shells, Jackfruit peel, *Borassus flabellifer* flower and corn cob, allowing for the utilization of a wide range of biomass sources [11–13]. In addition, recent interest has shifted toward microalgae owing to their unique advantages such as high photosynthetic efficiency, rapid growth rate, and minimal nutrient needs [14,15]. These characteristics make microalgae a promising renewable source of AC and other valuable products. Microalgae residues containing carbohydrates and proteins can be transformed into AC through pyrolysis followed by activation processes. Additionally, microalgae cultivation does not require arable land, making it a more sustainable option than terrestrial biomass sources [16]. Furthermore, microalgae can be cultivated using wastewater which adds to their environmental appeal by reducing their demand for freshwater resources. These advantages align with SDG 6 (Clean Water and Sanitation) and SDG 12 (Responsible Consumption and Production).

Althouh *Chlorella* and *Spirulina* are commonly studied for CO_2 adsorbent production, there is limited research on *Nannochloropsis gaditana*. *Nannochloropsis* is a microalga known for its application in wastewater treatment to adsorb heavy metals and dye [17,18]. Investigating the potential of *Nannochloropsis gaditana* residue obtained from lipid extraction as a feedstock for CO_2-optimized AC could fill this research gap and, offer a cost-effective and efficient alternative for industrial CO_2 capture applications. According to Huang's research, a significant amount of residue after lipid extraction from microalgae and is considered a process waste [19]. During biodiesel production, nearly 50 % of the biomass is generated as a by-product after the extraction of lipids, as microalgae usually contain up to 55 % of lipids [19]. Another study stated that microalgae residues after lipid extraction make up approximately 70 % of the dry weight of microalgae biomass and retain a significant amount of carbohydrates and proteins [20]. According to Toro Aedo et al. (2013), microalgae residues can range from 30 to 60 % of the dry microalgae weight because the lipid content can vary from 25 to 75 % depending on the type of strain. This phenomenon offers an opportunity to enhance resource efficiency by adopting the circular economy paradigm, which focuses on smart and sustainable use of resources. It aims to minimize resource extraction, waste generation, and emissions by promoting closed-loop systems that ensure that materials are effectively reused, recycled, and repurposed effectively [21]. Therefore, utilizing microalgae residues can promote circular economy by minimizing industrial waste.

This study aimed to produce activated carbon from *Nannochloropsis gaditana* microalgal residue. Chemical activation via potassium hydroxide (KOH) impregnation was used to increase the surface porosity of the activated carbon. A one-step carbonation and activation method was employed to reduce sample preparation time. The prepared activated carbon was then characterized for surface morphology, elemental analysis, surface functional groups, Brunauer-Emmett-Teller (BET) surface area, pore width, and total pore volume. In addition, the CO_2 adsorption performance of *N. gaditana* residue-derived activated carbon was evaluated at various CO_2 temperatures (25–55 °C) and inlet gas flow rates (200–400 mL/min) using breakthrough analysis. The data collected were also used for the kinetic study of the CO_2 adsorption behavior of *N. gaditana* residue-derived activated carbon. In addition, a cyclic CO_2 adsorption study was conducted to evaluate the stability and regeneration ability of the samples.

2. Materials and methods

2.1. Preparation of raw materials

Hydrochloric acid (≥99 %) and potassium hydroxide (≥99 %) were purchased from Sigma–Aldrich. Purified nitrogen (99.99 %) and carbon dioxide (99.80 %) were supplied by Alpha Gas Solution (Sdn). Bhd., Malaysia. *Nannochloropsis gaditana* residue was purchased from Xi'an Jenifer Technology Co.,Ltd., China. The residue was obtained by lipid extraction using ethanol solvent.

2.2. Preparation of activated carbon

The *Nannochloropsis gaditana* residue (NR) was directly impregnated with KOH (100 wt%) at a carbon-to-KOH mass ratio of 8:1 on a dry basis [22]. The KOH pellets were ground and thoroughly mixed with the microalgae-residue powder. The impregnated precursor was calcined in a furnace at 400 °C with a heating rate of 10 °C /min for 30 min [22]. The resulting carbon material was cooled to room temperature and then washed with 0.1 M hydrochloric acid and distilled water until reaching pH 7 [23]. Lastly, the washed sample was dried at 103 °C for 24 h [24] to produce black and dried *Nannochloropsis gaditana* residue-derived activated carbon (NRAC). The raw *Nannochloropsis gaditana* residue (NR) did not undergo carbonization or activation. The yield of NRAC ranged at 30–45 wt%.

2.3. Evaluation of CO_2 adsorption performance

A packed-bed CO_2 column custom–made by Berqat Engineering Sdn Bhd was used to study the breakthrough curve of CO_2 adsorption by activated carbon. The fixed-bed column was designed with a 15 mm inner diameter of 350 mm effective length. The column was filled with 35 g of NRAC adsorbent up to an effective bed height of 6 cm. The sample was then placed in the adsorption column, and pure N_2 gas was introduced to purge any residual CO_2 from the column. This step ensured that no CO_2 remained on the surface of the NRAC before starting the experiment. Flow meters were used to measure and control the flow of N_2 and CO_2, which entered from the bottom of the column. The gases were mixed upstream using a stainless-steel T-junction to achieve the desired inlet concentration of 15 vol% CO_2. The parameters for this study were the adsorption temperature and inlet CO_2 flow rate, whereas the variables of interest were CO_2 adsorption capacity and breakthrough time. The experiment was conducted at atmospheric pressure with an initial 15 vol% CO_2 concentration. The flow rates of N_2 and CO_2 were controlled in the feed stream to produce the desired CO_2 volumetric concentration. The adsorption performance of the prepared activated carbon was evaluated at different adsorption temperatures (22–55 °C) and inlet CO_2 flow rates (200–400 mL/min).

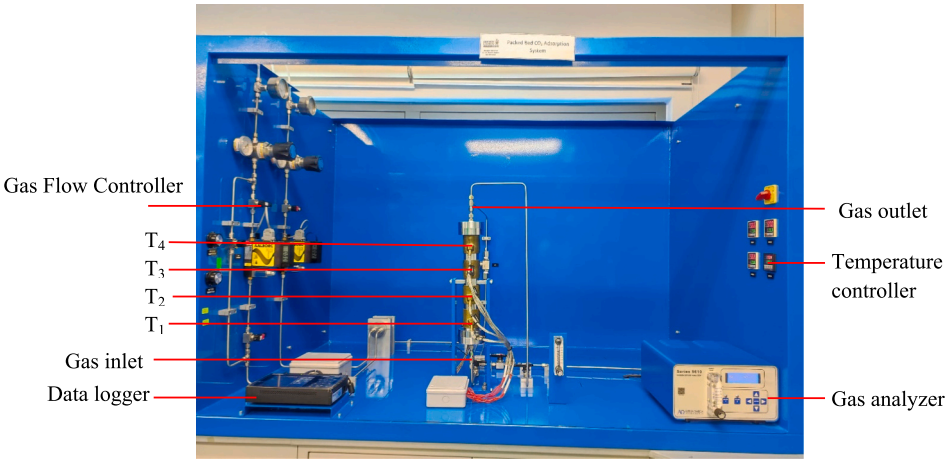

Fig. 1. Experimental set-up for CO_2 breakthrough analysis.

A CO_2 analyzer (Model: Alpha Omega Instruments Series 9610) was used to measure the CO_2 concentration at the column outlet at regular intervals of 60 s, and the measurements were recorded using a data logger (Model: Graphtec GL820). Non-dispersive infrared (NDIR) sensor was used in CO_2 analyzer that can detect up to 20 vol% and a resolution of ±0.1 vol%. The sampling data was taken continuously and direct from the outlet stream. The response time of the analyzer is less than 35 s. The experiment was continued until the outlet CO_2 concentration (C_t) was equal to the inlet CO_2 concentration (C_0). The breakthrough time, t_b was obtained from the graph of C_t/C_0 vs time. In this study, t_b was referred to when $C_t/C_0 = 0.05$ whereas the saturation time, t_s was when $C_t/C_0 = 1$. At t_s point, the adsorbent is completely saturated and may no longer adsorb the incoming CO_2 molecules. Fig. 1 shows the experimental set-up of a fixed-bed CO_2 adsorption unit for a breakthrough curve study.

2.4. Regeneration study

In the regeneration study, the adsorption procedure was performed in a manner similar to that of the breakthrough study. After the adsorbent reached saturation and t_s was obtained, desorption was performed where the gas flow was switched to pure N_2 at a flow rate of 200 mL/min to remove CO_2 completely from the column. The adsorbent was subjected to four consecutive adsorption-desorption cycles. The regeneration data were collected using a data logger at the end of the experiment and tabulated to analyze the stability of the NRAC.

2.5. Sample characterization

The surface morphology and elemental composition of the samples (NR and NRAC) were examined by Scanning Electron Microscopy (SEM) with Energy Dispersive X-ray Spectroscopy (EDX) (Model: Tescan VEGA-3, Brno, Czech Republic) at an accelerating voltage of 15 kV. The presence of surface functional groups in both samples was identified using Fourier Transform Infrared (FTIR) spectroscopy (Bruker, VERTEX 70v, Rosenheim, Germany). The surface area, total pore volume, and pore diameter of the samples were measured by nitrogen adsorption-desorption analysis at 77 K using a Micromeritics TriStar 3000 V6.06 A. Nitrogen adsorption isotherms were recorded over a relative pressure (p/p_o) range of 0.005–0.99. The surface area and average pore width were calculated using the Brunauer–Emmett–Teller (BET) method.

2.6. CO_2 adsorption kinetics

In this study, the experimental data for the CO_2 adsorption kinetics were fitted to pseudo-first-order (PFO) and pseudo-second-order (PSO) models. Lagergren's PFO kinetic model assumes that the adsorption rate is directly proportional to the number of free active sites available on the adsorbent surface [25]. In contrast, Ho and McKay stated that the rate of adsorption in PSO model is proportional to the square of the number of unoccupied active sites on the adsorbent surface [26]. The PSO model has been widely used to fit the kinetic rate data for the adsorption of metal ions, dyes, and other compounds from the liquid phase onto adsorbents [27], and has also been employed by many researchers to fit the kinetics data of CO_2 adsorption [25]. The non-linear forms of the PFO and PSO models are presented in Eq. (1) and Eq. (2), respectively:

$$q_t = q_e\left(1 - e^{-k_1^t}\right) \tag{1}$$

$$\frac{t}{q_t} = \frac{1}{k_2 q_e^2} + \frac{t}{q_e} \tag{2}$$

where q_e is the adsorption capacity of the adsorbent at equilibrium (mmol/g), q_t is the adsorption capacity of the adsorbent at time t (mmol/g), k_1 is the rate constant for PFO adsorption (min^{-1}), and k_2 is the rate constant for PSO adsorption (mmol/g. min), and t is time (min). Given the initial conditions $q_t = 0$ at $t = 0$.

3. Results and discussion

3.1. Material characterization

3.1.1. Surface functional groups

FTIR analysis provided insights into the surface functional groups of raw microalgae residue powder (NR), fresh AC (NRAC), and AC after CO_2 adsorption at flow rates of 200 mL/min (A1) and 400 mL/min (B1). In terms of O—H stretching, NR exhibited strong O—H stretching peaks at 3780 cm^{-1}, 3695 cm^{-1}, and 3433 cm^{-1}, which are attributed to hydroxyl (-OH) groups from water, polysaccharides, or proteins in the microalgae cell walls [28]. The NRAC retained these O—H bands at 3780 cm^{-1}, 3684 cm^{-1}, and 3452 cm^{-1}, indicating surface hydroxyls were still present even after calcination at 400 °C. This might be due to the addition of -OH groups from the alkaline activating agent (KOH), incomplete dehydration or the formation of new -OH groups on the carbon surface [29]. Another reason is the presence of residual lipids in the biomass after calcination. Previous research has identified the lipid peak in the 3550–3200 cm^{-1} region resulting from the symmetrical and asymmetrical stretching of CH_2 groups [30]. Some researchers have suggested the presence of O—H, carboxylic acids, alcohols, and phenolic groups in the regions between 3100 and 3700 cm^{-1} [31,32]. After 200 mL/min CO_2 adsorption (A1), new O—H bands appeared at 3747 cm^{-1}, 3679 cm^{-1}, 3610 cm^{-1}, and 3393 cm^{-1}, suggesting additional

interactions between CO_2 and surface hydroxyls, possibly forming bicarbonate or carbonate-like species. However, hydroxyl groups were significantly reduced, where only a single broad peak at 3181 cm^{-1} remained in 400 mL/min CO_2 adsorption (B1). This suggests either the displacement of weakly bound water molecules or chemical transformations reducing the hydroxyl content at higher CO_2 flow rates.

Next, for C—H stretching in aliphatic hydrocarbons, NR showed peaks at 2919 cm^{-1} and 2853 cm^{-1}, indicating the presence of alkane groups, likely from residual lipids or fatty acids in the biomass [30]. These peaks persisted in NRAC at 2919 cm^{-1} and 2850 cm^{-1}, implying that some aliphatic structures survived the activation at 400 °C. In A1, CO_2 adsorption did not significantly alter these groups as the aliphatic C—H peaks remained at 2924 cm^{-1} and 2853 cm^{-1}. However, in B1, the C—H stretching bands disappeared, indicating that at higher CO_2 exposures, the aliphatic chains were either oxidized or rearranged, which caused them to be eliminated from the surface.

For C═O stretching in carbonyl, carboxyl, ester, and lactone groups, the raw sample exhibited a carbonyl (C=O) stretching peak at 1731 cm^{-1}, which could be attributed to esters or carboxyl groups naturally present in microalgae-derived lipids (triglycerides) and fatty acids [30]. Similarly, a previous study indicated that peaks within the 1700–1800 cm^{-1} range also confirmed an increased concentration of fatty acids [33]. In NRAC, the similar appearance of the C═O peak at 1736 cm^{-1} suggested that these carbonyl functionalities remained after calcination. This aligns with the FTIR results of a previous study on microalgae-based activated carbon, prepared using KOH activation, which revealed the presence of C═O bonds, indicating a higher concentration of oxygen-containing functional groups. These groups can significantly enhance CO_2 adsorption capacity [34]. The presence of oxygen-containing functional groups (such as hydroxyl, carboxyl, and carbonyl) enhanced the CO_2 adsorption capacity because they increase the surface polarity and provide active sites for CO_2 molecules to interact through stronger dipole-quadrupole interactions or hydrogen bonding, thus improving the adsorption performance [35]. After 200 mL/min CO_2 adsorption (A1), two C═O bands appeared at 1741 cm^{-1} and 1661 cm^{-1}. This indicated the formation of new surface-bound carbonyl species because of the CO_2 interaction, forming lactone, quinone or carboxyl functionalities [36]. In B1, the carbonyl peaks shifted to 1821 cm^{-1} and 1677 cm^{-1}, which could correspond to anhydride-like species [37]. This increase in intensity suggests that an increase in CO_2 exposure led to further restructuring of the surface-bound carbonyl groups.

In addition, NR showed a C═C stretching peak at 1599 cm^{-1}, which is possibly due to aromatic rings from lignin-derived compounds or polyphenolic structures [38,39]. Fresh NRAC displayed a peak at 1547 cm^{-1} which showed some retention of aromatic structures after activation, even with slight modifications. Similarly, A1 retained C═C peaks at 1561 cm^{-1} and 1514 cm^{-1} even after CO_2 exposure. However, the C═C stretching peaks in B1 disappeared completely. The absence of C═C stretching in B1 combined with the presence of a new band near 1821 cm^{-1} and 1677 cm^{-1} proved that aromatic structures were transformed into quinone-like species under high CO_2 adsorption conditions [36]. This suggests that prolonged CO_2 exposure disrupted the conjugated π-electron system of the aromatic rings.

C—O stretching in carboxyl, phenol, and ether groups typically ranges from 800 to 1300 cm^{-1} [32]. The raw microalgae powder (NR) exhibited C—O stretching at 1219 cm^{-1} and 1075 cm^{-1}, which could be attributed to ether, phenolic, or ester groups naturally present in the biomass. In fresh NRAC, these peaks slightly shifted to 1217 cm^{-1} and 1087 cm^{-1} because of the structural modifications from thermal activation. A1 showed a peak at 1231 cm^{-1} indicating the possible formation of new oxygen-containing surface groups through CO_2 interaction. The presence of C—O stretching in B1 at 1170 cm^{-1} suggested that the surface underwent further oxidation that may form ether groups that are highly stable under high temperatures [36].

The NR and NRAC samples exhibited aromatic C—H bending vibrations at approximately 670 cm^{-1}. This illustrates that the aromaticity of the structure is preserved even after activation. In the A1 sample, this peak shifted to 705 cm^{-1}, which showed some degree of modification in the aromatic rings while retaining their structure. The expected aromatic C—H bending vibrations were absent in sample B1, but new peaks appeared at 558 and 476 cm^{-1}, indicating a breakdown of aromaticity. This transformation suggests that at a higher CO_2 adsorption rate, the aromatic rings may have undergone chemical alterations, which led to the formation of quinone-like or other oxygenated surface species. The observed spectral changes indicate that the increased CO_2 flow could have induced structural modifications, resulting in the conversion of aromatic structures into oxygen-containing functional groups.

Table 1
Surface functional groups on the adsorbent surface.

Assignment	Wavenumber (cm^{-1})			
	NR	Fresh NRAC	After 200 mL/min CO_2 Adsorption (A1)	After 400 mL/min CO_2 Adsorption (B1)
O-H stretching (hydroxyl groups)	3780, 3695, 3433	3780, 3684, 3452	3747, 3679, 3610, 3393	3181
C-H stretching (aliphatic hydrocarbons)	2918, 2853	2919, 2850	2924, 2853	–
C=O stretching (carbonyl, carboxyl, ester, lactone)	1731	1736	1741, 1661	1821, 1677
C=C stretching (aromatic, conjugated C=O groups)	1599	1547	1561, 1514	–
C-O stretching (carboxyl, phenol, ether)	1219, 1075	1217, 1087	1231	1170
Bending vibrations (C—H, aromatic rings, others)	669	667	705	558, 476

The comparison of FTIR spectra before and after CO_2 adsorption reveals spectral changes that indicate the active participation of the functional groups of the adsorbents in the adsorption process [37]. Overall, the FTIR results suggest that KOH activation at 400 °C successfully introduced oxygen-containing functional groups, including hydroxyl, carbonyl, and ether groups, contributing to the CO_2 adsorption capacity [40]. In addition, the presence of alkanes, phenols, and alcohols helped trap pollutants on the activated carbon [37]. The adsorption process at 25 °C led to the formation of surface-bound carbonate or carboxylate species and promoted more extensive modifications in surface chemistry at higher CO_2 flow rates (400 mL/min). The presence of stronger carbonyl peaks in B1 suggests that higher CO_2 flow rates facilitate greater interactions between CO_2 and the active sites on the AC surface, potentially enhancing chemisorption mechanisms. Meanwhile, the retention of hydroxyl groups in A1 suggests a higher proportion of physisorption at lower CO_2 flow rate (200 mL/min). These findings highlight the importance of oxygenated functional groups in CO_2 adsorption and indicate that varying CO_2 flow rates can influence the adsorption mechanism and surface chemistry of activated carbon derived from microalgal residues.

Table 1 summarizes the functional groups on the adsorbent surface. Fig. 2 shows the FTIR spectra of raw microalgae residue (NR), microalgae residue-derived activated carbon before CO_2 adsorption (Fresh NRAC), microalgae residue-derived activated carbon after CO_2 adsorption at 200 mL/min (A1), and microalgae-derived activated carbon after CO_2 adsorption at 400 mL/min (B1).

3.1.2. Surface morphology

Scanning electron microscopy (SEM) was used to analyze the surface morphology of raw microalgae residue powder (NR) and microalgae

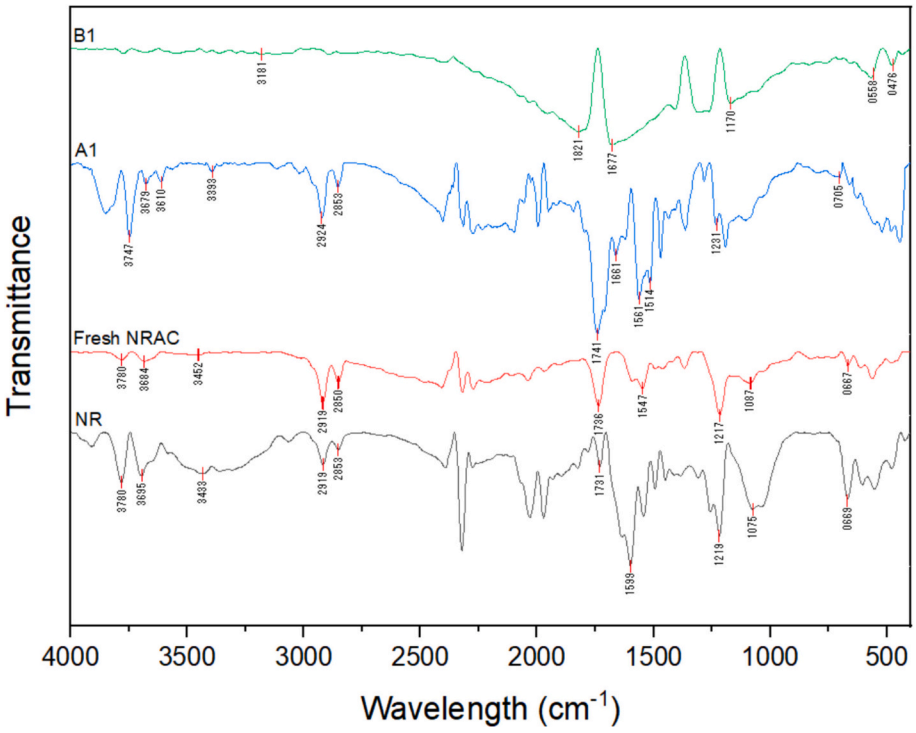

Fig. 2. FTIR spectrum analysis of raw microalgae residue (NR), microalgae residue-derived activated carbon before CO_2 adsorption (Fresh NRAC), NRAC after CO_2 adsorption at 200 mL/min (A1), NRAC after CO_2 adsorption at 400 mL/min (B1).

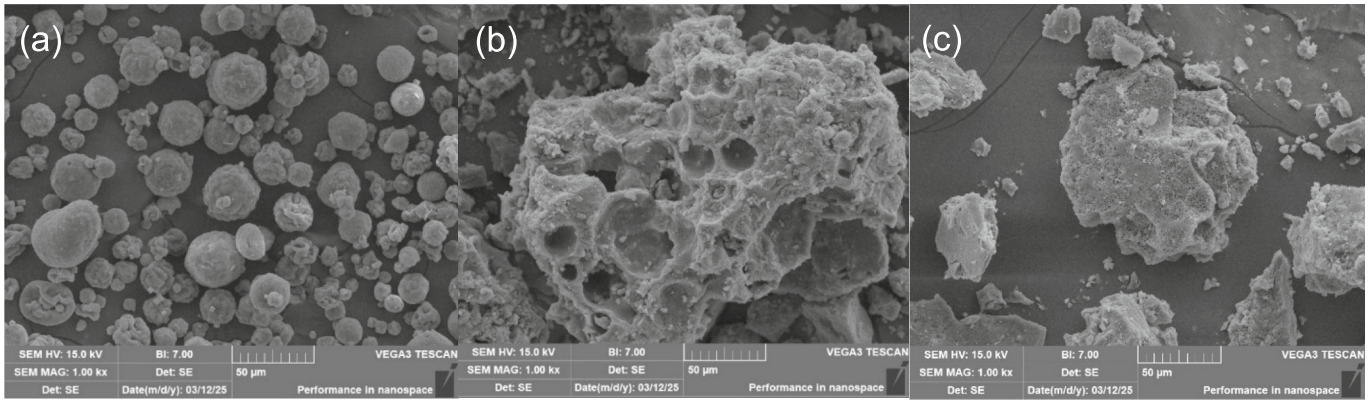

Fig. 3. SEM analysis of (a) raw microalgae residue (NR), (b) fresh NRAC and (c) NRAC after CO_2 adsorption.

residue-derived AC (NRAC) before and after CO_2 adsorption. Fig. 3 shows different magnifications of the raw microalgae residue powder and activated carbon. As shown in Fig. 3 (a), NR exhibited irregular spherical structures and a relatively smooth surface with no cavities. Similar results have been reported for the surface morphology of raw microalgae [41]. After carbonization and activation, the surface morphology of fresh NRAC changed significantly. Fig. 3 (b) shows the formation of a well-developed porous and fragmented structure, which indicates successful activation. A rough surface with irregular cavities and pores was expected to increase the surface area and facilitate CO_2 adsorption. The heterogeneous surfaces with developed micropores and mesopores were likely attributed to the dehydration effect of KOH during activation. This process disrupts the C–O–C and C—C bonds and releases potassium oxide (K_2O), hydrogen gas (H_2), and potassium carbonate (K_2CO_3), which contribute to pore development [42]. The possible reactions that occur during KOH activation are as follows:

$$4KOH + C \rightarrow K_2O + 2H_2 + K_2CO_3 \quad (3)$$

$$2KOH \rightarrow K_2O + H_2O \quad (4)$$

$$C + H_2O \rightarrow CO + H_2 \quad (5)$$

$$CO + H_2O \rightarrow CO_2 + H_2 \quad (6)$$

$$K_2O + CO_2 \rightarrow K_2CO_3 \quad (7)$$

Fig. 3 (c) shows that after CO_2 adsorption, the NRAC exhibited further morphological changes. The surface appeared to have less visible pore structures than the fresh NRAC. This suggests that CO_2 adsorption might have led to structural modifications, potentially through interactions between the functional groups of activated carbon and adsorbed gas molecules. The presence of crystalline or agglomerated deposits indicates the formation of stable surface complexes or carbonate-related structures. Additionally, some pores were blocked, possibly due to the accumulation of adsorbed CO_2 molecules.

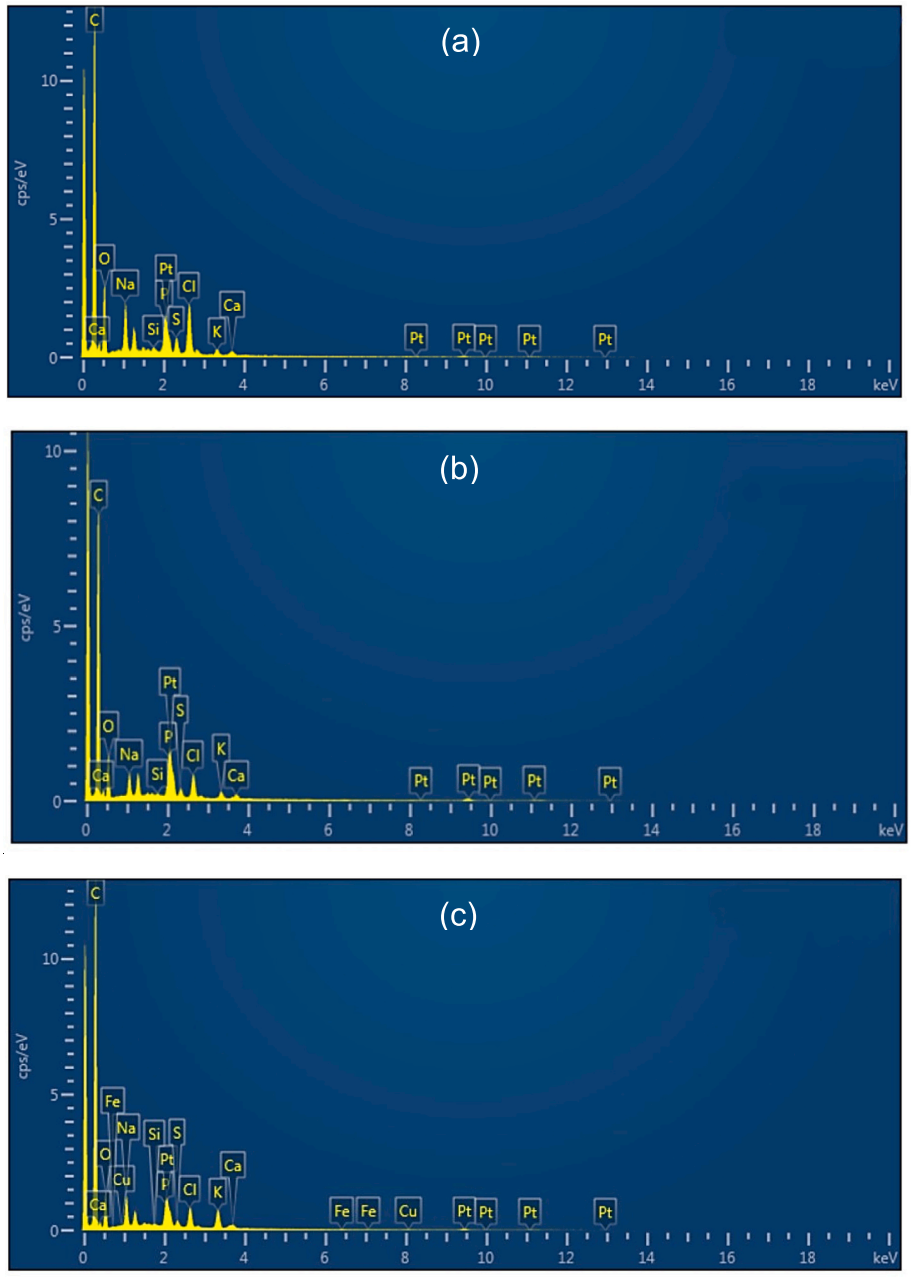

Fig. 4. EDX spectrum of (a) raw microalgae residue (b) fresh NRAC (c) NRAC after CO_2 adsorption.

3.1.3. Elemental composition

EDX analysis provides insights into the elemental composition changes of the raw microalgae residue, fresh NRAC, and used NRAC after CO_2 adsorption as shown in Fig. 4. The results showed that the carbon content in this study was relatively higher than those reported in the literature, for example, 34.8 % and 43.47 % for *Scenedesmus* and *Nannochloropsis* residues, respectively [43,44]. The carbon content increased from 73.23 % in the raw microalgae residue to 76.78 % in fresh NRAC and 78.69 % in NRAC. This shows the successful carbonization of NR and potential surface modifications in NRAC after CO_2 adsorption. High carbon content facilitated the formation of aromatic compound, carboxyl and carbonyl groups which enhanced the physisorption of CO_2 on NRAC [45]. This is because more condensed aromatic rings provide extended π-systems that enhances the interaction energy between CO_2 and the carbon surface [46]. During CO_2 adsorption, some CO_2 molecules might be physically or chemically adsorbed onto AC, and some unstable oxygen-containing functional groups such as O—H might transform into more stable carbon-oxygen structures, such as quinones, lactones, or anhydrides. As these situations occur, the relative oxygen content might decrease, while the proportion of carbon-bound species increases, resulting in a higher detected carbon content on the AC surface [47,48]. In contrast, the oxygen content decreased from 18.92 % in the raw microalgae residue to 14.11 % in the NRAC used, suggesting the removal of oxygenated functional groups during KOH activation [22]. In addition, the decrease in oxygen content after CO_2 adsorption might imply the transformation of certain oxygen-containing species through interactions with CO_2. Anhydrides or lactones formed in fresh NRAC may be converted into CO_2 during adsorption, leading to a loss of oxygen content [49].

The chlorine content decreased from 2.62 % in NR to 1.40 % in the used NRAC. This might be due to volatilization during thermal treatment or leaching during activation. In addition, the increase in potassium content in fresh NRAC could be attributed to the reaction between acidic functional groups such as carboxyl and phenolic groups, and basic

Table 2
EDX analysis of raw microalgae residue, fresh NRAC, and NRAC after CO_2 adsorption.

Element	Weight %		
	Raw	Fresh NRAC	Used NRAC
C	73.23	76.78	78.69
O	18.92	16.17	14.11
Na	2.00	1.29	1.68
Cl	2.62	1.62	1.40
Mg	0.79	1.00	0.65
P	0.77	1.36	0.71
S	0.71	0.50	0.34
K	0.41	0.65	1.76
Ca	0.32	0.43	0.36
Al	0.12	0.11	0.10
Si	0.12	0.09	0.07

KOH, which resulted in the formation of potassium salts [50]. On the other hand, potassium increased from 0.41 % to 1.76 %, possibly because of the surface adsorption of residual KOH during the activation process, forming stable potassium [51]. Furthermore, the increase in the P content in fresh NRAC could be attributed to the activation process, where carbonization enhanced the retention of phosphorus by eliminating other volatile elements [52]. Both aluminum (Al) and silicon (Si) contents were relatively low and were considered negligible. This aligns with the mineral composition found in another study of *N. gaditana* species [53].

Furthermore, the presence of Mg in the raw *N. gaditana* residue could lead to magnesium carbonate ($MgCO_3$) formation during carbonization and activation [54]. This is because Mg-containing minerals such as MgO, in the *N. gaditana* residue could react with the CO_2 released from the decomposition of organic matter during carbonization. This supports the increase in Mg content in the observed fresh NRAC as some $MgCO_3$ might remain on the activated carbon surface. The decrease in Mg after CO_2 adsorption might be due to the formation of new functional groups such as quinones, lactones, or anhydrides, which could alter the surface chemistry. A similar case can be applied to Ca, in which calcium carbonate ($CaCO_3$) is formed after activation and carbonization. In addition, the decline in sulfur content in fresh NRAC after KOH activation could be explained by alkali-promoted sulfur release, where organic sulfur compounds decompose, followed by the formation and removal of inorganic sulfur salts and SO_2 gas [55]. Lastly, sodium (Na) showed an increase in used NRAC, which indicated that some sodium species participate in CO_2 adsorption [56,57].

3.1.4. Surface area, total pore volume and pore size

Brunauer–Emmett–Teller (BET) analysis was conducted to evaluate the specific surface area, pore size, and pore volume of the synthesized activated carbon. As shown in Table 2, the BET results of NR and NRAC were compared with those of the other microalgae-derived adsorbents. The NRAC exhibited a BET surface area of 296.96 m^2/g with an average pore diameter of 2.26 nm, and a total pore volume of 0.17 cm^3/g. The average pore diameter falls within the mesoporous range (2–50 nm), indicating that the activation of *Nannochloropsis gaditana* residue using KOH at 400 °C for 30 min successfully produced a mesoporous material, similar to the other adsorbents in Table 3.

The BET-specific surface area of NRAC was mostly lower than that of other microalgae-derived adsorbents, especially the KOH-activated *Nannochloropsis* AC reported by Masoumi and Dalai, which achieved a significantly higher surface area of 2099 m^2/g with a larger pore diameter of 5.90 nm [32]. This may be attributed to the higher activation temperatures (525–825 °C) employed in their study, which promoted greater pore development and higher porosity. Additionally, their higher total pore volume of 1.2 cm^3/g compared to that of NRAC's 0.17 cm^3/g indicated a more extensive pore network. Other study also showed direct proportional relationship between activation temperature and porosity (BET surface area and micropore volume) [58]. A lower surface area (844 m^2/g) and total pore volume (0.5 cm^3/g) were also reported by Masoumi and Dalai when a lower activation temperature and a smaller amount of KOH were used [32]. Similarly, the relatively low BET surface area of 296.96 m^2/g observed for NRAC can be attributed to the mild activation conditions employed in this study, specifically at 400 °C with a KOH-to-biomass ratio of 1:8. Study has shown that lower carbonization temperatures can lead to the formation of oxygen-rich carbon structures, which may enhance adsorption capacity [59]. Additionally, other research indicates that effective carbon activation can still be achieved under relatively mild conditions [60].

However, the NRAC produced in this study still demonstrated a competitive performance compared to other algae-based adsorbents. For instance, N-doped microwave activated carbon derived from Spirulina

Table 3
BET surface area, pore diameter, and total pore volume of different adsorbent.

Adsorbent precursor	Type of adsorbent	Activating agent	S_{BET} (m^2/g)	Average pore diameter (nm)	Total pore volume (cm^3/g)	Micropore volume (cm^3/g)	Adsorption capacity (mmol/g CO_2)	References
Chlorella	Biochar	KOH	5.0	3.00	0.01	–	–	[34]
Chlorella	N-doped microwave AC	KOH (1:1)	396.5	2.24	0.22	–	3.44	[34]
Chlorella	N-doped microwave AC	KOH (2:1)	602.8	2.57	0.37	–	4.21	[34]
Spirulina	Biochar	KOH	5.7	5.23	0.01	–	–	[34]
Spirulina	N-doped microwave AC	KOH (1:1)	189.7	2.85	0.14	–	3.09	[34]
Spirulina	N-doped microwave AC	KOH (2:1)	510.3	2.74	0.33	–	3.57	[34]
Nannochloropsis gladina	AC	KOH (1.5:1, 675 °C)	2099	5.90	1.2	0.58	–	[32]
Nannochloropsis gladina	AC	KOH (1:2, 550 °C)	844	12.70	0.5	0.22	–	[32]
Nannochloropsis gladina	AC	H_3PO_4	406	10.90	0.28	0.14	–	[32]
Nannochloropsis gaditana residue (NR)	Raw	–	5.45	2.98	0.01	0.006	12.94 (cm^3/g N_2)	This study
Nannochloropsis gaditana residue (NRAC)	AC	KOH	296.96	2.26	0.17	0.13	0.55 (mmol/g CO_2) 112.16 (cm^3/g N_2)	This study

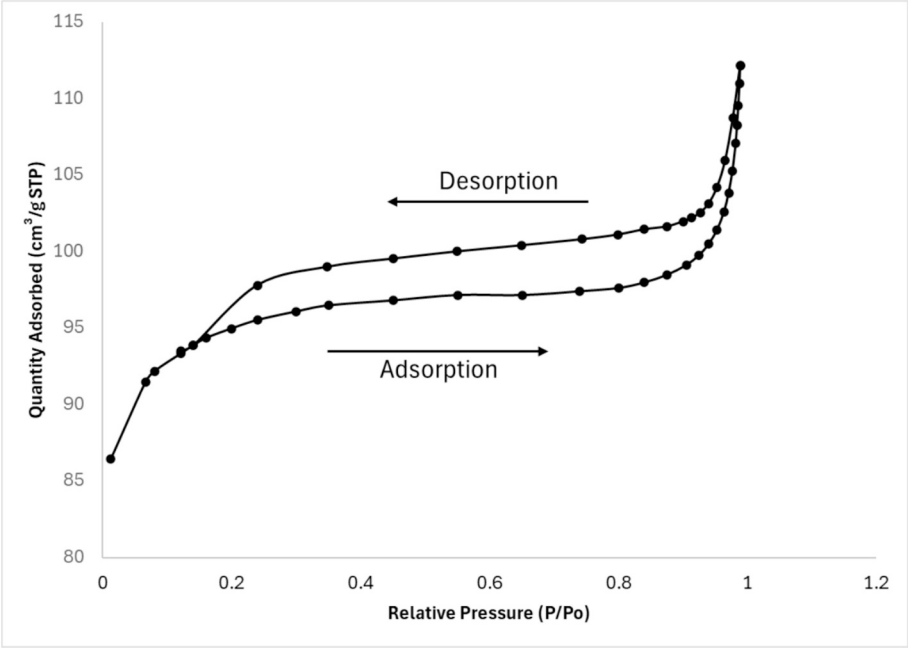

Fig. 5. Isotherm of KOH-activated NRAC from *N.gaditana* residue.

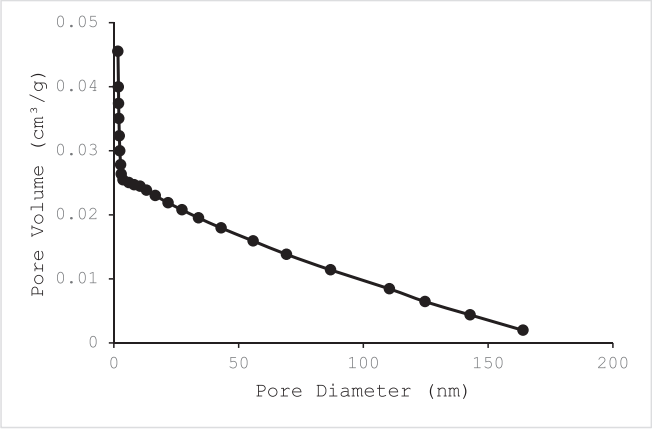

Fig. 6. Pore size distribution curve of NRAC.

by Shi & Liu recorded a BET surface area of 189.7 m^2/g, which is lower than that of NRAC [34]. Similarly, KOH-activated Chlorella microwave carbon (396.5 m^2/g, 2.24 nm pore diameter, 0.22 cm^3/g pore volume) is comparable with NRAC having a higher surface area but similar mesopore structure. Overall, these comparisons highlight that although NRAC exhibited a lower surface area owing to milder activation conditions (more sustainable), the adsorbent still achieved a well-developed mesoporous structure. Although the average pore diameter of NRAC was 2.26 nm, BET reported 0.13 cm^3/g of micropore volume which accounted for 76.47 % of the total pore volume. These micropores significantly contributed to the CO_2 adsorption by NRAC because CO_2 molecules have small kinetic diameter of 0.33 nm [61]. Mesopores were serving as gas diffusion channels to transport CO_2 molecules to adjacent microporous regions. Comparing NR and NRAC, BET showed that both total pore volume and micropores volume are directly proportional to the adsorption capacity of the examined samples.

The nitrogen adsorption-desorption isotherm of the KOH-activated *Nannochloropsis gaditana* residue-derived activated carbon shown in Fig. 5 exhibits a Type IV profile with an H4-type hysteresis loop. According to the International Union of Pure Applied Chemistry (IUPAC) classification, Type IV isotherms are characteristic of well-developed mesoporous materials and are distinguished from Type II by the presence of a hysteresis loop associated with capillary condensation within the pores [62–64]. This aligns with the measured average pore diameter of 2.26 nm, further confirming the mesoporous structure of the activated carbon. Fig. 6 shows the pore size distribution of NRAC.

The Type IV isotherm indicates that adsorption primarily occurs within the micropores at lower relative pressures, where the formation of a "knee" in the isotherm represents the completion of monolayer adsorption. As the relative pressure increased further, the appearance of a plateau reflected the development of multilayer adsorption across the pore surfaces. At higher relative pressures, the sharp increase in the adsorbed volume was attributed to capillary condensation within the mesopores [65]. The H4 hysteresis loop indicates the existence of asymmetric, narrow, and slit-shaped pore structures. Similar results were reported by [66] in their study of activated carbon derived from hemp bast fibers.

3.2. *Effect of inlet gas flow rate*

The effects of the inlet CO_2 flow rate on the breakthrough time and adsorption capacity were investigated. Fig. 7 shows that an increase in the inlet CO_2 flow rate from 200 to 400 mL/min resulted in a shorter breakthrough time when temperatures were kept constant at 25, 40 and 55 °C, respectively. This was because more CO_2 molecules were introduced into the column, causing faster saturation of the surface of the activated carbon [67]. Similar results were reported by Hanh and Danish [67,68]. Furthermore, the mass transfer zone (MTZ) became narrower at a higher gas flow rate due to faster adsorption at the initial stage. This phenomenon limited the time available for CO_2 molecules to diffuse into deeper layers of the adsorbent, resulting in an earlier breakthrough [69].

The increase in the gas flow rate theoretically results in higher adsorption capacity owing to the presence of more CO_2 molecules. The amount of CO_2 adsorbed per adsorbent increased with an increasing CO_2 flow rate at 25°, as shown in Fig. 8. The adsorption capacity increased from 0.39 to 0.55 mmol/g when the flow rate increased from 200 to 400 mL/min. A similar trend was observed at both 40 and 55 °C. As the gas flow rate increased, the residence time of the gas within the activated carbon decreased. However, a higher flow rate induced turbulence

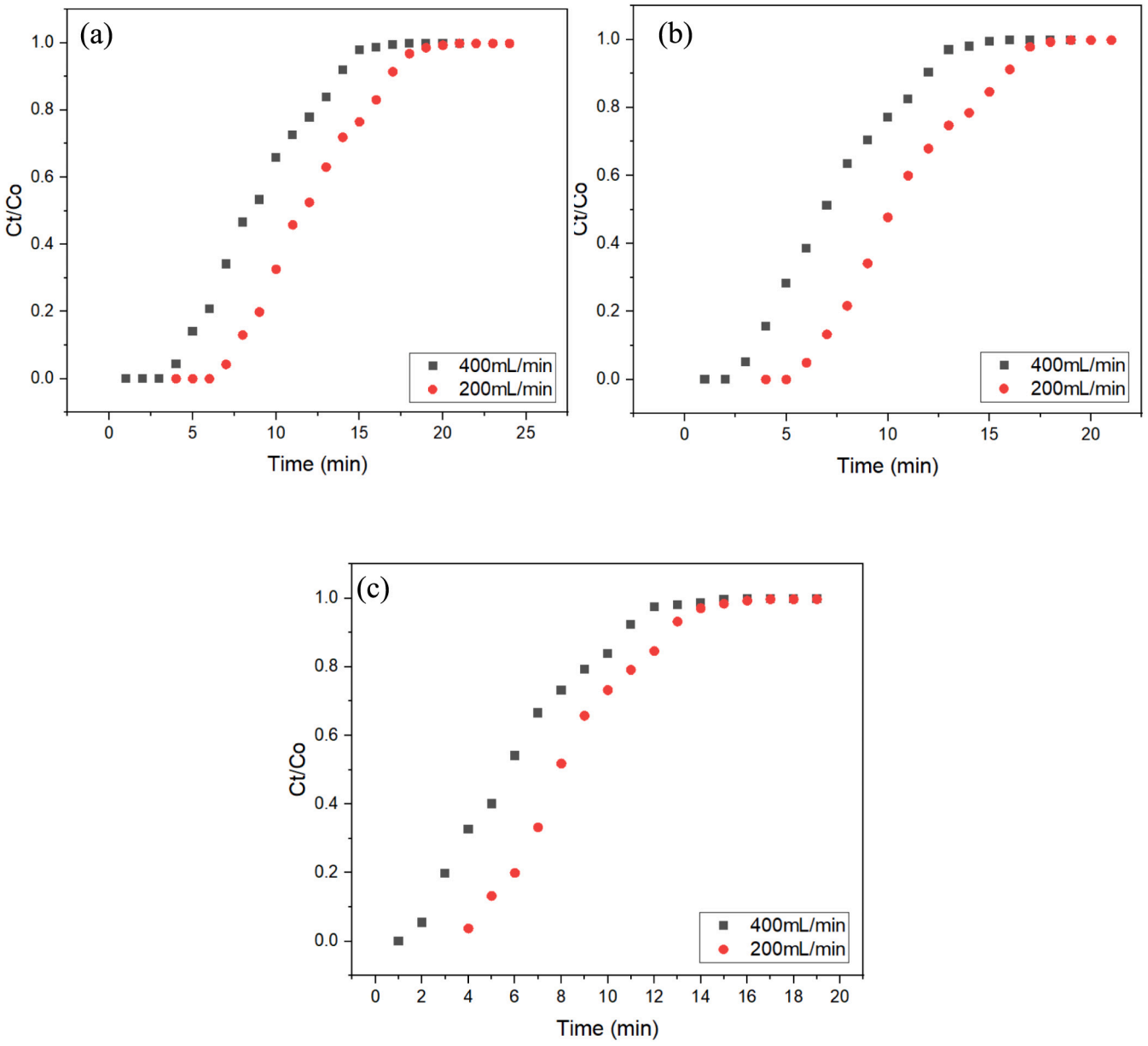

Fig. 7. Effect of inlet flow rate on breakthrough time at (a) 25 °C, (b) 40 °C and (c) 55 °C.

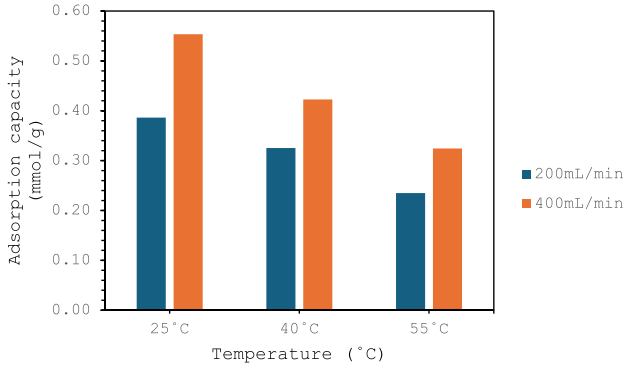

Fig. 8. Effect of inlet flow rate on adsorption capacity.

within the column, which enhanced the mass transfer between the CO_2 molecules and the activated carbon. More CO_2 molecules were effectively transferred from the bulk gas phase to the gas-solid boundary layer, resulting in an improvement in the mass transfer coefficient. This phenomenon was demonstrated by Gül et al. [70] and Guo et al. [71].

In contrast, other studies have shown that lower flow rates result in better CO_2 adsorption capacity. For instance, Suratman et al. [72] found that the adsorption capacity decreased after the optimum gas flow rate because the interaction between the gas and adsorbent decreased when the gas flow rate was too high. The gas molecules moved too fast and did not have sufficient time to be effectively adsorbed by the activated carbon. When the number of available adsorption sites remained unchanged, additional CO_2 molecules could no longer interact with the saturated active sites; hence, the adsorption capacity remained unchanged despite the increase in the inlet CO_2 flow rate, as illustrated in the literature [71]. At higher flow rates, the adsorption sites on the activated carbon might become saturated more quickly, leading to a plateau in the adsorption capacity. A previous study [73] observed that increasing the flow rate decreased the breakthrough time, indicating a

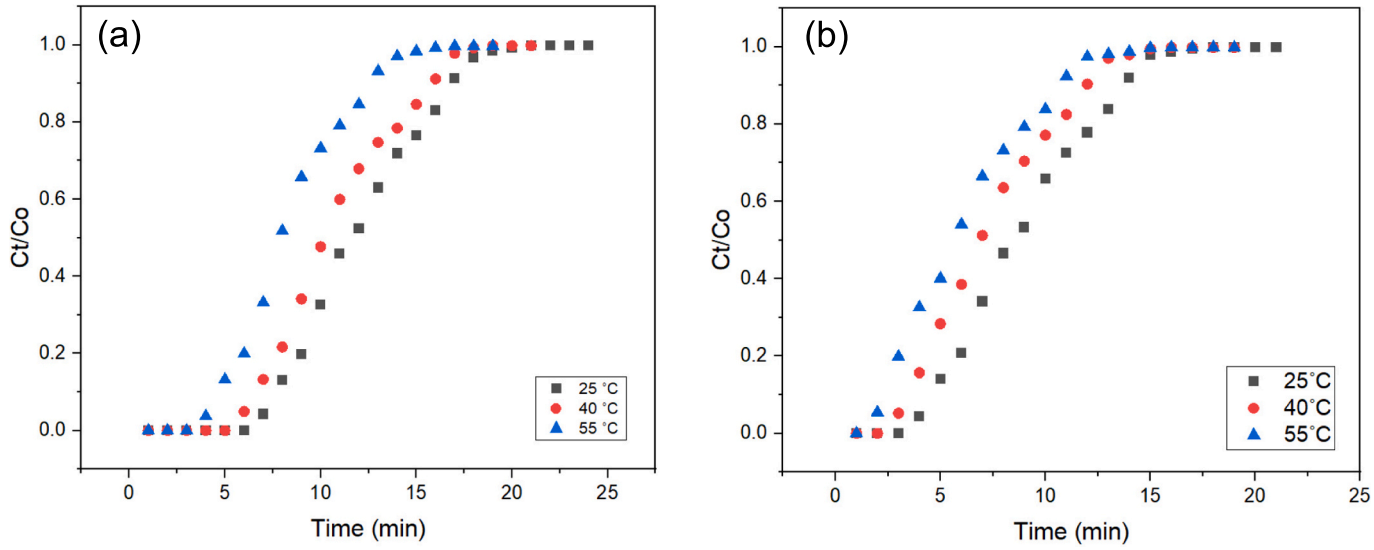

Fig. 9. Effect of temperature on breakthrough time at (a) 200 mL/min and (b) 400 mL/min.

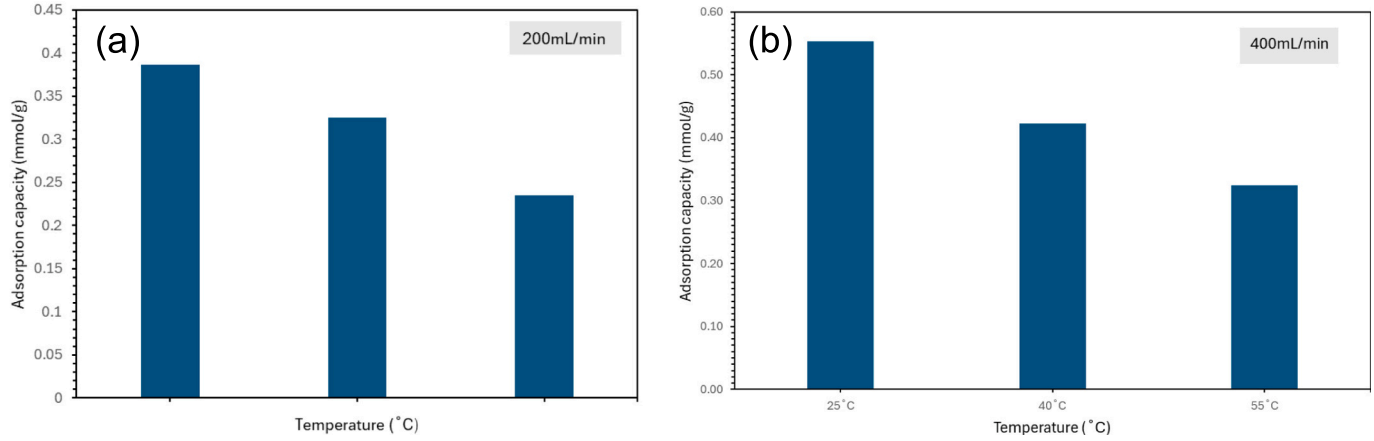

Fig. 10. Effect of temperature on adsorption capacity under (a) 200 mL/min and (b) 400 mL/min flow rates.

faster adsorbent saturation. Another study showed that reducing the gas flow rate could increase the contact time and enhance the mass transfer between CO_2 molecules and activated carbon, leading to a higher adsorption capacity [37].

3.3. *Effect of CO_2 temperature*

The CO_2 adsorption experiment was conducted at three different temperatures (25, 40, and 55 °C) to examine the effect temperature on the adsorption capacity of the activated carbon and its breakthrough time. Fig. 9 (a) illustrates that the breakthrough time decreased from 7 to 4 min with increasing column temperature from 25 to 55 °C under a constant CO_2 flow rate of 200 mL/min. Moreover, Fig. 9 (b) shows a similar trend at 400 mL/min, where the breakthrough time decreased to 4, 3 and 2 min at 25, 40, and 55 °C, respectively. These results align with the findings of previous studies [25,74], as higher temperatures led to faster desorption of CO_2 molecules, which then led to shorter breakthrough times. Fig. 10 shows the adsorption capacity of 0.39, 0.33, and 0.24 mmol/g at 25, 40 and 55 °C, respectively when using a constant of 200 mL/min and 15 vol% CO_2. Similarly, declined adsorption capacities of 0.55, 0.42, and 0.32 mmol/g were observed at 25, 40 and 55 °C, respectively, with a constant flow rate of 400 mL/min and 15 vol% CO_2. The decrease in adsorption capacity with increasing column temperature was caused by the increase in the kinetic energy of the CO_2 molecules at higher temperatures, which could overcome the binding force, thus causing them to desorb from the activated carbon. Another reason was the exothermic nature of adsorption, where the high temperature shifted the equilibrium to the reverse side of the process, which meant that desorption would occur. Eventually, the instability of CO_2 molecules owing to the increase in energy supply led to a faster breakthrough and lower adsorption capacity [75]. Based on the results obtained, the process can be expected to involve physical adsorption between the CO_2 molecules and the activated carbon surface [74]. The reported effects of temperature on adsorption capacity in this work align with previous studies reported by other researchers [76–78].

The highest adsorption capacity of 0.55 mmol/g was observed at the lowest temperature, 25 °C and the highest flow rate, at 400 mL/min, in Fig. 10(b), with corresponding longer breakthrough time in Fig. 9(b), indicating an increased uptake of CO_2 under these conditions [68]. These are attributed to the combined effects of (i) lowering the temperature which reduces the CO_2 desorption rate and (ii) increasing the gas flow rates, which introduces more CO_2 molecules to the process and enhances the CO_2 adsorption efficiency. On the other hand, adsorption capacity for all temperatures were expected to decrease because less CO_2 molecules available at lower concentrations, such as 10 vol% or below, leads to smaller uptake capacity. This was proven by Ibrahim et.al [79], where approximately 15 % reduction of adsorption capacity when CO_2 concentration decreased from 13.725 vol% to 10 vol%. Besides, author

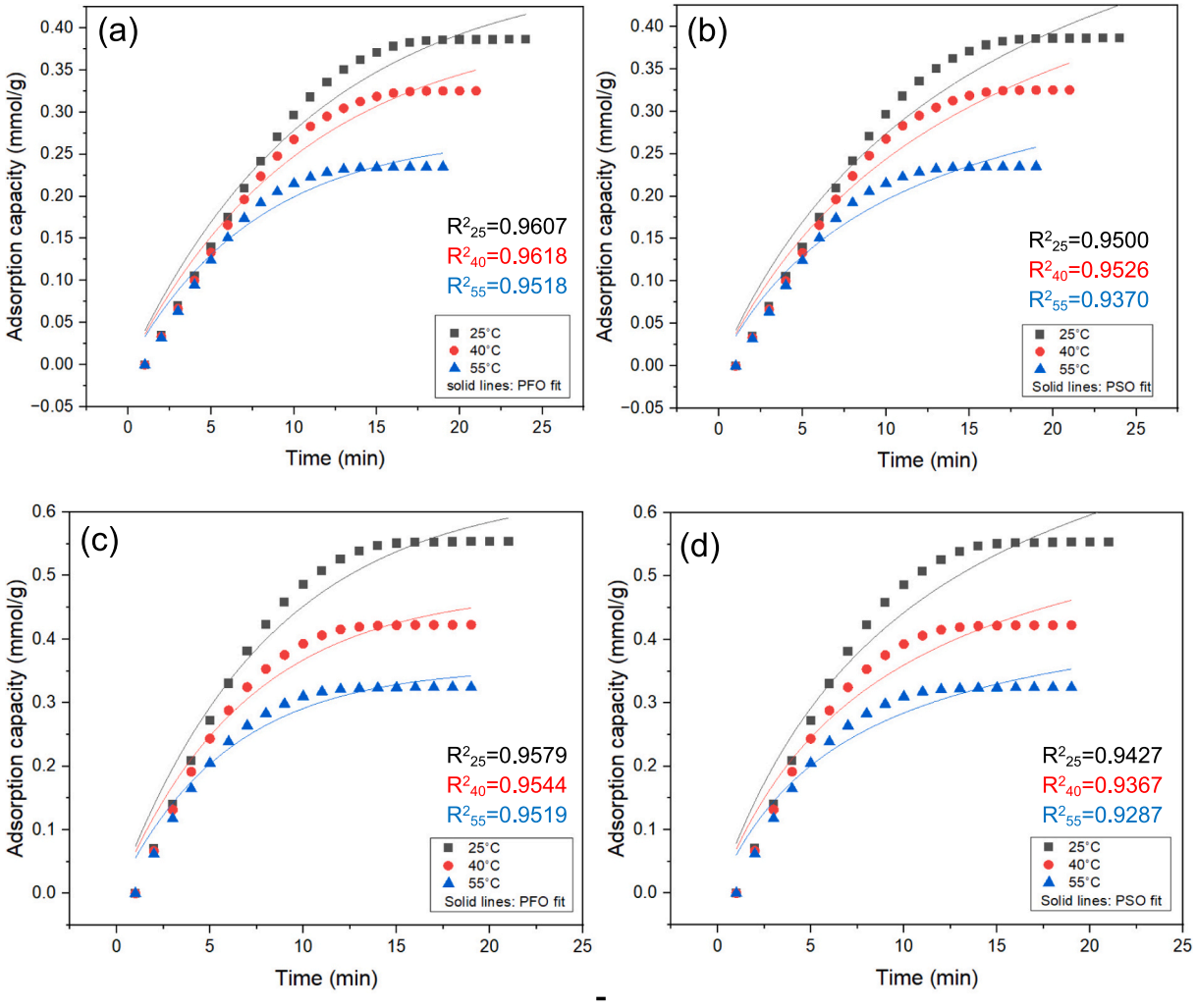

Fig. 11. Adsorption kinetics curve of CO_2 on NRAC under 200 mL/min flow rate, fitted to (a) PFO and (b) PSO, and under 400 mL/min flow rate, fitted to (c) PFO and (d) PSO.

Table 4
Pseudo first and second order kinetics model parameters of CO2 adsorption on NRAC.

Flow rate (mL/min)	Temperature (°C)	Pseudo-first-order			Pseudo-second-order		
		q_e (mmol/g)	k_1 (min^{-1})	R^2	q_e (mmol/g)	k_2 (mmol/g.min)	R^2
200	25	0.4714	0.0893	0.9607	0.7041	0.0903	0.9500
	40	0.4066	0.0939	0.9618	0.6184	0.1052	0.9526
	55	0.2750	0.1291	0.9518	0.3987	0.2416	0.9370
400	25	0.6391	0.1228	0.9579	0.9142	0.1026	0.9427
	40	0.4794	0.1454	0.9544	0.6750	0.1691	0.9367
	55	0.3565	0.1695	0.9519	0.4846	0.2927	0.9287

reported the CO_2 adsorption amount decreased by 6 % for flue gas mixture (CO_2, NO, N_2). Further study on the effect of CO_2 concentration and flue gas mixtures are recommended.

3.4. Kinetics of adsorption

The kinetics of CO_2 adsorption by NRAC was fitted to PFO and PSO using non-linear equations (Eqs. (1) & (2)), which can reduce approximation errors and provide a better representation of the reaction mechanism, and are compared based on the respective R^2 values. Fig. 11 shows the curves of non-linear CO_2 adsorption kinetics at different inlet CO_2 flow rates and temperatures.

A higher correlation coefficient, R^2, indicate that the data fit the kinetic model more accurately. As shown in Table 4, The PFO model exhibited a superior fit to the CO_2 adsorption data compared with the PSO model, especially at 293 K or when the inlet gas flow rate is lower. This suggests that the adsorption process was physisorption, which involved weak van der Waals forces or physical interactions rather than chemical bonding. Lagergen's PFO adsorption kinetics model, also known as the linear driving force (LDF) model, suggests that the adsorption rate is proportional to the number of unoccupied sites and is commonly applied when physical adsorption is dominant [80,81]. This process is typically fast and reversible [82].

The adsorption rate constant (k_1) of the PFO model in this study

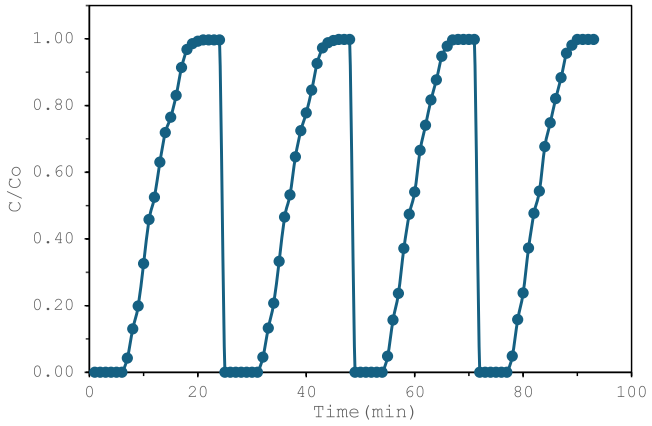

Fig. 12. Regeneration of NRAC at 25 °C, 15 vol% CO_2 and 200 mL/min flow rate.

increased with increasing temperature because of the enhanced mobility and interaction of CO_2 molecules with the activated carbon surface. This contradicts the research conducted by Liu and Singh, where their adsorption rate constants in PFO decreased with increasing temperature [25,81]. Previous studies have suggested that the CO_2 adsorption process on activated carbon is primarily controlled by intra-particle diffusion, which refers to the movement of CO_2 molecules within the pores of the adsorbent. In this study, when the temperature increased, the CO_2 molecules gained more kinetic energy, leading to more frequent and forceful collisions with the adsorbent surface. This increased interaction enhanced the adsorption rate, resulting in a higher k_1 value. A similar trend was reported by Saha et al. [83] in research on the adsorption of methyl orange onto chitosan adsorbents, although PSO was identified as the best fit in their case. Because the correlation coefficients (R^2) of PFO and PSO models in this study are relatively close, it is likely that both chemisorption and physisorption are involved in CO_2 adsorption by NRAC, with physisorption being the dominant mechanism.

In addition, the CO_2 adsorption capacity decreased as the temperature increased at both flow rates of 200 and 400 mL/min. Desorption is expected at higher temperatures, which reduces the overall adsorption capacity. This phenomenon further confirms the physisorption mechanism. In line with this study, other studies on CO_2 adsorption also discovered that the PFO kinetic model was better at describing the adsorption process than PSO using olive waste-derived AC and amine-functionalized KIT-6 [81,84].

3.5. Cyclic adsorption/desorption performance

The stability of an adsorbent is crucial for its successful practical application in an industrial setting. An effective CO_2 adsorbent must retain its adsorption performance over multiple adsorption-desorption cycles to ensure long-term functionality and reusability. The stability of the adsorbent was assessed based on the decline in the adsorption performance (%) over multiple cycles of adsorption-regeneration testing. As illustrated in Figs. 12 and 13, NRAC demonstrated strong adsorption capacity and stability throughout several adsorption-desorption cycles. In the second cycle, the adsorption capacity increased from 0.39 to 0.41 mmol/g, likely due to moisture loss from the NRAC surface during the initial regeneration step, resulting in more available active sites for CO_2 adsorption.

A slight decline was observed in the third cycle, with the adsorption capacity decreasing back to 0.38 mmol/g and remaining constant through the fourth cycle. This indicates that no significant changes occurred in the mass transfer region, confirmed the stability of the NRAC adsorbent. This structural stability was due to carbon-rich structure where strong cross-linking occurred between the crystallites, making the AC resisted pore collapse [85]. A similar trend was observed and reported by other researchers and also in Liu and Yu's study, where a 6.5 % decrease in adsorption capacity after 10 cycles was still considered relatively stable [81,86,87].

4. Conclusion

This study aimed to produce activated carbon from microalgae residues after lipid extraction and evaluate its CO_2 adsorption performance through breakthrough curve experiments. Activated carbon was successfully produced by one-step KOH activation and carbonization of *Nannochloropsis gaditana* residue with a carbon-to-KOH ratio of 8:1. Carbonization was performed at 400 °C for 30 min. The characterization results revealed that the NRAC sorbent had a rough, complex surface with irregularly shaped pores developed as a result of chemical

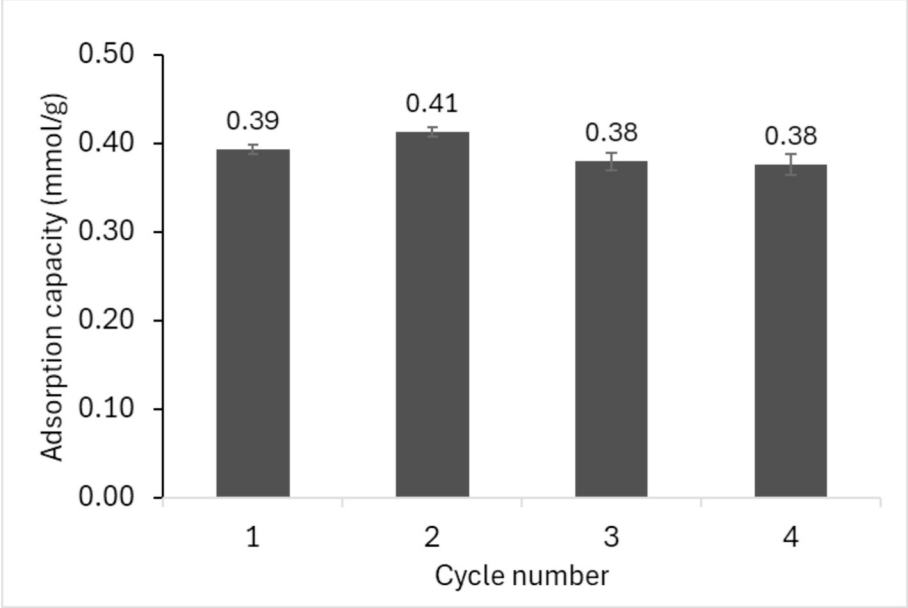

Fig. 13. NRAC adsorption capacity in several adsorption–desorption cycles.

activation with KOH, while the raw microalgae residue (NR) exhibited a smooth surface without obvious pore structures. EDX analysis also proved the successful treatment of NRAC with an increase in the carbon content compared to NR. The presence of oxygen-containing surface functional groups such as OH, C—O, and C═O was confirmed in the FTIR spectra. BET analysis showed an increase in the specific surface area of NRAC (296.96 m^2/g) compared to NR (5.45m^2/g). Moreover, NRAC had the longest breakthrough time at the lowest temperature (25 °C) and inlet gas flow rate (200 mL/min). The highest adsorption capacity of 0.55 mmol/g was recorded at 25 °C and 400 mL/min as the lower temperature can reduce the desorption of CO_2 molecules from the adsorbent surface, whereas a higher flow rate allows more CO_2 molecules to enter the adsorption column. In addition, the regeneration study demonstrated that NRAC maintained a stable performance over four adsorption-desorption cycles. According to the kinetic data, the PFO model provided the best fit for the adsorption of CO_2 on the NRAC adsorbent. The observed decrease in adsorption capacity with increasing temperature supported the exothermic nature of the process and suggested that physisorption was the dominant mechanism for CO_2 adsorption using NRAC.

Data access statement

Research data supporting this publication are available from the NN repository at located at www.NNN.org/download/.

CRediT authorship contribution statement

Low Yi Chian: Writing – original draft, Methodology, Investigation, Formal analysis, Data curation, Conceptualization. **Umi Fazara Md Ali:** Writing – review & editing, Supervision, Project administration, Methodology, Investigation, Funding acquisition, Data curation, Conceptualization. **Farihahusnah Hussin:** Writing – review & editing, Formal analysis, Conceptualization. **Mohamed Kheireddine Aroua:** Writing – review & editing, Visualization, Validation, Resources, Conceptualization. **Naimah Ibrahim:** Writing – review & editing, Resources, Project administration, Investigation. **Mohd Azmier Ahmad:** Writing – review & editing, Visualization, Validation, Resources.

Ethical compliance

All procedures performed in studies involving human participants were in accordance with the ethical standards of the institutional and/or national research committee and with the 1964 Helsinki Declaration and its later amendments or comparable ethical standards.

Declaration of competing interest

The authors declare that they have no affiliations with or involvement in any organization or entity with any financial interest in the subject matter or materials discussed in this manuscript.

Acknowledgements

The authors would like to express heartfelt gratitude to the Uni-PRIMA research grant (9001-00763) for its valuable financial support, which significantly contributed to the success of this study. We also thank Mohammad Fahmi Ramli and Mohamad Zaim Mohamad Zain for their assistance in the laboratory.

Data availability

No data was used for the research described in the article.

References

[1] Malaysia, Malaysia First NDC (Updated Submission) | UNFCCC, 2024 [Online]. Available: https://unfccc.int/documents/497775.
[2] WMO, Greenhouse Gas Concentrations Surge Again to New Record in 2023, World Meteorological Organization, 2024 [Online]. Available: https://wmo.int/news/media-centre/greenhouse-gas-concentrations-surge-again-new-record-2023.
[3] A.A. Abd, M.R. Othman, J. Kim, A review on application of activated carbons for carbon dioxide capture: present performance, preparation, and surface modification for further improvement, Environ. Sci. Pollut. Res. 28 (32) (2021) 43329–43364, https://doi.org/10.1007/s11356-021-15121-9.
[4] D.Y.C. Leung, G. Caramanna, M.M. Maroto-Valer, An overview of current status of carbon dioxide capture and storage technologies, Renew. Sustain. Energy Rev. 39 (2014) 426–443, https://doi.org/10.1016/j.rser.2014.07.093.
[5] UNFCC, Malaysia NDC Updated Submission to UNFCCC July 2021 final.pdf, 2024 [Online]. Available: https://unfccc.int/sites/default/files/NDC/2022-06/Malaysia%20NDC%20Updated%20Submission%20to%20UNFCCC%20July%202021%20final.pdf.
[6] SCM, National Sustainability Reporting Framework | Securities Commission Malaysia, 2024 [Online]. Available: https://www.sc.com.my/nsrf.
[7] H. Yang, et al., Progress in carbon dioxide separation and capture: a review, J. Environ. Sci. 20 (1) (2008) 14–27, https://doi.org/10.1016/S1001-0742(08)60002-9.
[8] L.S. Tan, A.M. Shariff, K.K. Lau, M.A. Bustam, Factors affecting CO2 absorption efficiency in packed column: a review, J. Ind. Eng. Chem. 18 (6) (2012) 1874–1883, https://doi.org/10.1016/j.jiec.2012.05.013.
[9] Y. Mochizuki, J. Bud, E. Byambajav, N. Tsubouchi, Pore properties and CO2 adsorption performance of activated carbon prepared from various carbonaceous materials, Carbon Resources Conversion (2024) 100237, https://doi.org/10.1016/j.crcon.2024.100237.
[10] M.Z. Hossain, M.B.I. Chowdhury, M.Z. Hossain, M.B.I. Chowdhury, Biobased activated carbon and its application, IntechOpen, 2024, https://doi.org/10.5772/intechopen.1008374.
[11] U. Tyagi, N. Anand, Sustainable and low-cost biomass derived adsorbents for the removal of toxic contaminants from wastewater: approaches and future perspective, Waste Manag. Bull. 2 (2) (2024) 308–325, https://doi.org/10.1016/j.wmb.2024.05.010.
[12] F.R. Christopher, N.A. Hamid, CO2 adsorption using Hydrochar prepared from jackfruit Peel, in: R.K. Agarwal (Ed.), Proceedings of the 8th International Conference on Manufacturing, Material and Metallurgical Engineering (ICMMME) 2024, Springer Nature Switzerland, Cham, 2025, pp. 201–207, https://doi.org/10.1007/978-3-031-78295-4_22.
[13] N.T. Tonu, et al., Fabrication of waste biomass-derived KOH activated carbon for enhanced CO2 capture, New J. Chem. 48 (48) (2024) 20212–20224, https://doi.org/10.1039/D4NJ04495A.
[14] A. Vilén, P. Laurell, R. Vahala, Comparative life cycle assessment of activated carbon production from various raw materials, J. Environ. Manage. 324 (2022) 116356, https://doi.org/10.1016/j.jenvman.2022.116356.
[15] M. Férez, F. Barceló, Á. Cortés, A. Gomis, E. Fernández, Production of activated carbon from microalgae, 2008.
[16] Green gold: harnessing non-arable lands for sustainable algae cultivation, in: Algae Processing, 2024 [Online]. Available: https://algaeprocessing.com/green-gold-harnessing-non-arable-lands-for-sustainable-algae-cultivation.
[17] B. Buhani, T. Wijayanti, S. Suharso, Sumadi, Application of Modified Green Algae *Nannochloropsis* sp. as Adsorbent in the Sequential Adsorption of Methylene Blue and Cu(II) Cations in Solution, 2020, https://doi.org/10.21203/rs.3.rs-64063/v1.
[18] A. Zuorro, G. Maffei, R. Lavecchia, Kinetic modeling of azo dye adsorption on non-living cells of *Nannochloropsis oceanica*, J. Environ. Chem. Eng. 5 (4) (2017) 4121–4127, https://doi.org/10.1016/j.jece.2017.07.078.
[19] Z. Huang, et al., Valorisation of microalgae residues after lipid extraction: pyrolysis characteristics for biofuel production, Biochem. Eng. J. 179 (2022) 108330, https://doi.org/10.1016/j.bej.2021.108330.
[20] G. Li, et al., Enhancing bioenergy production from the raw and defatted microalgal biomass using wastewater as the cultivation medium, Bioengineering 9, no. 11, Art. no. 11 (2022), https://doi.org/10.3390/bioengineering9110637.
[21] B. Suárez-Eiroa, E. Fernández, G. Méndez-Martínez, D. Soto-Oñate, Operational principles of circular economy for sustainable development: linking theory and practice, J. Clean. Prod. 214 (2019) 952–961, https://doi.org/10.1016/j.jclepro.2018.12.271.
[22] W. Chen, et al., Insight into KOH activation mechanism during biomass pyrolysis: chemical reactions between O-containing groups and KOH, Appl. Energy 278 (2020) 115730, https://doi.org/10.1016/j.apenergy.2020.115730.
[23] T. Yang, A.C. Lua, Characteristics of activated carbons prepared from pistachio-nut shells by potassium hydroxide activation, Microporous Mesoporous Mater. 63 (1) (2003) 113–124, https://doi.org/10.1016/S1387-1811(03)00456-6.
[24] O. Oginni, K. Singh, G. Oporto, B. Dawson-Andoh, L. McDonald, E. Sabolsky, Influence of one-step and two-step KOH activation on activated carbon characteristics, Bioresource Technology Reports 7 (2019) 100266, https://doi.org/10.1016/j.biteb.2019.100266.
[25] V.K. Singh, E.A. Kumar, Comparative studies on CO2 adsorption kinetics by solid adsorbents, Energy Procedia 90 (2016) 316–325, https://doi.org/10.1016/j.egypro.2016.11.199.
[26] Y.S. Ho, G. McKay, Pseudo-second order model for sorption processes, Process Biochem. 34 (5) (1999) 451–465, https://doi.org/10.1016/S0032-9592(98)00112-5.

[27] M.A. Hubbe, S. Azizian, S. Douven, Implications of apparent pseudo-second-order adsorption kinetics onto cellulosic materials: a review, BioResources 14 (3) (2019) 7582–7626, https://doi.org/10.15376/biores.14.3.7582-7626.
[28] J. Sreńscek-Nazzal, et al., The increase of the micoporosity and CO2 adsorption capacity of the commercial activated carbon CWZ-22 by KOH treatment, in: Microporous and Mesoporous Materials, IntechOpen, 2016, https://doi.org/10.5772/63672.
[29] G. Özsin, M. Kilic, E. Apaydın-Varol, A. Pütün, Chemically activated carbon production from agricultural waste of chickpea and its application for heavy metal adsorption: equilibrium, kinetic, and thermodynamic studies, Appl. Water Sci. 9 (2019), https://doi.org/10.1007/s13201-019-0942-8.
[30] M. Arif, Y. Li, M.M. El-Dalatony, C. Zhang, X. Li, E.-S. Salama, A complete characterization of microalgal biomass through FTIR/TGA/CHNS analysis: an approach for biofuel generation and nutrients removal, Renew. Energy 163 (2021) 1973–1982, https://doi.org/10.1016/j.renene.2020.10.066.
[31] S. Acevedo, L. Giraldo, J.C. Moreno-Piraján, Adsorption of CO2 on activated carbons prepared by chemical activation with cupric nitrate, ACS Omega 5 (18) (2020) 10423–10432, https://doi.org/10.1021/acsomega.0c00342.
[32] S. Masoumi, A.K. Dalai, Optimized production and characterization of highly porous activated carbon from algal-derived hydrochar, J. Clean. Prod. 263 (2020) 121427, https://doi.org/10.1016/j.jclepro.2020.121427.
[33] R. Kothari, V.V. Pathak, V. Kumar, D.P. Singh, Experimental study for growth potential of unicellular alga *Chlorella pyrenoidosa* on dairy waste water: an integrated approach for treatment and biofuel production, Bioresour. Technol. 116 (2012) 466–470, https://doi.org/10.1016/j.biortech.2012.03.121.
[34] S. Shi, Y. Liu, Nitrogen-doped activated carbons derived from microalgae pyrolysis by-products by microwave/KOH activation for CO2 adsorption, Fuel 306 (2021) 121762, https://doi.org/10.1016/j.fuel.2021.121762.
[35] B. Liu, H. Li, X. Ma, R. Chen, S. Wang, L. Li, The synergistic effect of oxygen-containing functional groups on CO2 adsorption by the glucose–potassium citrate-derived activated carbon, RSC Adv. 8 (68) (2018) 38965–38973, https://doi.org/10.1039/c8ra05523h.
[36] J. Jaramillo, P.M. Álvarez, V. Gómez-Serrano, Oxidation of activated carbon by dry and wet methods: surface chemistry and textural modifications, Fuel Process. Technol. 91 (11) (2010) 1768–1775, https://doi.org/10.1016/j.fuproc.2010.07.018.
[37] S.O. Akpasi, Y.M. Isa, Effect of operating variables on CO2 adsorption capacity of activated carbon, kaolinite, and activated carbon – kaolinite composite adsorbent, Water-Energy Nexus 5 (2022) 21–28, https://doi.org/10.1016/j.wen.2022.08.001.
[38] C.C. Azubuike, M.N. Allemann, J.K. Michener, Microbial assimilation of lignin-derived aromatic compounds and conversion to value-added products, Curr. Opin. Microbiol. 65 (2022) 64–72, https://doi.org/10.1016/j.mib.2021.10.014.
[39] A. Shafique, T. Fazal, H.M.U. Ayub, Q. Abbas, F. Ashraf, Valorization of algal biomass to synthesize visible-light driven gC3N4-biochar composite for dye degradation: tuning of optical-electronic properties and persulfate-photocatalytic mechanistic insights, Journal of Hazardous Materials Advances 18 (2025) 100683, https://doi.org/10.1016/j.hazadv.2025.100683.
[40] C. Qiu, L. Jiang, Y. Gao, L. Sheng, Effects of oxygen-containing functional groups on carbon materials in supercapacitors: a review, Mater. Des. 230 (2023) 111952, https://doi.org/10.1016/j.matdes.2023.111952.
[41] K. Maliutina, A. Tahmasebi, J. Yu, Effects of pressure on morphology and structure of bio-char from pressurized entrained-flow pyrolysis of microalgae, Data Brief 18 (2018) 422–431, https://doi.org/10.1016/j.dib.2018.03.048.
[42] M. Tsarpali, J.N. Kuhn, G.P. Philippidis, Activated carbon production from algal biochar: chemical activation and feasibility analysis, Fuel Communications 19 (2024) 100115, https://doi.org/10.1016/j.jfueco.2024.100115.
[43] A. Kumar, et al., Co-pyrolysis of microalgae residue and sewage sludge: an in-depth characterization of kinetics, drivers, and gas-oil-char behaviors, J. Anal. Appl. Pyrolysis 179 (2024) 106438, https://doi.org/10.1016/j.jaap.2024.106438.
[44] J.L. Ramos-Suárez, N. Carreras, Use of microalgae residues for biogas production, Chem. Eng. J. 242 (2014) 86–95, https://doi.org/10.1016/j.cej.2013.12.053.
[45] G. Li, et al., Adsorption of CO2/CH4 on the aromatic rings and oxygen groups of coal based on in-situ diffuse reflectance FTIR, Gas Science and Engineering 130 (2024) 205440, https://doi.org/10.1016/j.jgsce.2024.205440.
[46] L. Chen, F. Cao, H. Sun, Ab initio study of the π–π interactions between CO2 and benzene, pyridine, and pyrrole, Int. J. Quantum Chem. 113 (20) (2013) 2261–2266, https://doi.org/10.1002/qua.24444.
[47] C. Zhang, et al., Surface oxygen-containing functional groups: a key tradeoff in carbon-based energy storage devices, Chem. Eng. J. 505 (2025) 159162, https://doi.org/10.1016/j.cej.2024.159162.
[48] H. Zhao, D. Zhao, J. Ye, P. Wang, M. Chai, Z. Li, Directional oxygen functionalization by defect in different metamorphic-grade coal-derived carbon materials for sodium storage, Energy Environ. Mater. 5 (1) (2022) 313–320, https://doi.org/10.1002/eem2.12178.
[49] G. de la Puente, J.J. Pis, J.A. Menéndez, P. Grange, Thermal stability of oxygenated functions in activated carbons, J. Anal. Appl. Pyrolysis 43 (2) (1997) 125–138, https://doi.org/10.1016/S0165-2370(97)00060-0.
[50] M. Danish, R. Hashim, M. Rafatullah, O. Sulaiman, A. Ahmad, Characterization of Activated Carbon from *Acacia Mangium* Wood Prepared in the Presence of Acid Base Activating aGents, Presented at the Bioresources, 2011, https://doi.org/10.15376/biores.6.3.3019-3033.
[51] T.-D. Hoang, Y. Liu, M.T. Le, Performance of CO2 adsorption on modified activated carbons derived from Okara powder waste: impacts of Ammonia impregnation, Processes 12, no. 9, Art. no. 9 (2024), https://doi.org/10.3390/pr12092024.
[52] S. Zhang, et al., Pyrolytic and hydrothermal carbonization affect the transformation of phosphorus fractions in the biochar and hydrochar derived from organic materials: a meta-analysis study, Sci. Total Environ. 906 (2024) 167418, https://doi.org/10.1016/j.scitotenv.2023.167418.
[53] G. Di Lena, et al., Chemical characterization and nutritional evaluation of microalgal biomass from large-scale production: a comparative study of five species, Eur. Food Res. Technol. 246 (2) (2020) 323–332, https://doi.org/10.1007/s00217-019-03346-5.
[54] K.N. Wahyusi, A.S. Ferdian, M.A. Panangian, I.N. Puspitawati, Synthesis of magnesium carbonate with bittern raw material with carbon dioxide gas injection in packing column, Nusantara Science and Technology Proceedings (2021) 1–6, https://doi.org/10.11594/nstp.2021.1401.
[55] J. Shan, J. Huang, J. Li, G. Li, J. Zhao, Y. Fang, Insight into transformation of sulfur species during KOH activation of high sulfur petroleum coke, Fuel 215 (2018) 258–265, https://doi.org/10.1016/j.fuel.2017.09.117.
[56] J. Guo, C. Nie, S. Li, N. Yan, P. Guo, Z. Liu, Revealing the CO2 adsorption blocking mechanism in flexible low-silica small-pore zeolites via three-dimensional electron diffraction, Chem. Commun. 61 (12) (2025) 2568–2571, https://doi.org/10.1039/D4CC06791F.
[57] D. Newsome, S. Gunawan, G. Baron, J. Denayer, M.-O. Coppens, Adsorption of CO2 and N2 in Na–ZSM-5: effects of Na+ and Al content studied by grand canonical Monte Carlo simulations and experiments, Adsorption 20 (1) (2014) 157–171, https://doi.org/10.1007/s10450-013-9560-1.
[58] F. de Gomes Ferreira Paula, I. Campello-Gómez, P.F.R. Ortega, F. Rodríguez-Reinoso, M. Martínez-Escandell, J. Silvestre-Albero, Structural flexibility in activated carbon materials prepared under harsh activation conditions, Materials (Basel) 12 (12) (2019) 1988, https://doi.org/10.3390/ma12121988.
[59] R.L. Zornitta, K.M. Barcelos, F.G.E. Nogueira, L.A.M. Ruotolo, Understanding the mechanism of carbonization and KOH activation of polyaniline leading to enhanced electrosorption performance, Carbon 156 (2020) 346–358, https://doi.org/10.1016/j.carbon.2019.09.058.
[60] G. Chen, N.Y. Kim, N. Kun, (PDF) Creating pores on graphene platelets by low-temperature KOH activation for enhanced electrochemical performance, ResearchGate (2025), https://doi.org/10.1002/smll.201503855.
[61] N. Mehio, S. Dai, D. Jiang, Quantum mechanical basis for kinetic diameters of small gaseous molecules, J. Phys. Chem. A 118 (6) (2014) 1150–1154, https://doi.org/10.1021/jp412588f.
[62] M.A. Al-Ghouti, D.A. Da'ana, Guidelines for the use and interpretation of adsorption isotherm models: a review, J. Hazard. Mater. 393 (2020) 122383, https://doi.org/10.1016/j.jhazmat.2020.122383.
[63] C. Bläker, J. Muthmann, C. Pasel, D. Bathen, Characterization of activated carbon adsorbents – state of the art and novel approaches, ChemBioEng Reviews 6 (4) (2019) 119–138, https://doi.org/10.1002/cben.201900008.
[64] V. Gómez-Serrano, C.M. González-García, M.L. González-Martín, Nitrogen adsorption isotherms on carbonaceous materials. Comparison of BET and Langmuir surface areas, Powder Technol. 116 (1) (2001) 103–108, https://doi.org/10.1016/S0032-5910(00)00367-3.
[65] A.G.M. Shoaib, A. El-Sikaily, A. El Nemr, A.E.-D.A. Mohamed, A.A. Hassan, Preparation and characterization of highly surface area activated carbons followed type IV from marine red alga (*Pterocladia capillacea*) by zinc chloride activation, Biomass Conv. Biorefin. 12 (6) (2022) 2253–2265, https://doi.org/10.1007/s13399-020-00760-8.
[66] M.Z. Hossain, et al., High-surface-area mesoporous activated carbon from hemp bast fiber using hydrothermal processing, C 4 (3) (2018) 3, https://doi.org/10.3390/c4030038.
[67] N.T.D. Hanh, et al., Estimation and error analysis of breakthrough curves for CO2 adsorption in packed-bed columns using polyethyleneimine-modified NaY zeolite under ambient conditions by single-component adsorption models, J. Taiwan Inst. Chem. Eng. 164 (2024) 105681, https://doi.org/10.1016/j.jtice.2024.105681.
[68] M. Danish, V. Parthasarathy, M. Al Mesfer, Breakthrough Adsorption Study Using Activated Carbon and Molecular Sieve for CO2 Capture, 2021, https://doi.org/10.21203/rs.3.rs-323987/v1.
[69] M. Danish, V. Parthasarthy, M.K. Al Mesfer, Comparative study of CO2 capture by adsorption in sustainable date pits-derived porous activated carbon and molecular sieve, Int. J. Environ. Res. Public Health 18 (16) (2021) 16, https://doi.org/10.3390/ijerph18168497.
[70] A. Gül, U. Tezcan Un, Effect of temperature and gas flow rate on CO2 capture, Eur. J. Sustain. Dev. Res. 6 (2022) 181.
[71] B. Guo, J. Zhang, Y. Wang, X. Qiao, J. Xiang, Y. Jin, Study on CO2 adsorption capacity and kinetic mechanism of CO2 adsorbent prepared from fly ash, Energy 263 (2023) 125764, https://doi.org/10.1016/j.energy.2022.125764.
[72] A. Suratman, S. Suyanta, F. Veronica, Adsorption of carbon dioxide with nanofibers based on alginate/polyethylene oxide/triton X-100, Jan. 2020, pp. 53–63.
[73] A. ur Rehman, J.W. Baek, E. Rene, N. Sergienko, S. Behera, H. Park, Effect of process parameters influencing the chemical modification of activated carbon fiber for carbon dioxide removal, Process Saf. Environ. Prot. 118 (2018), https://doi.org/10.1016/j.psep.2018.07.004.
[74] S. García, M.V. Gil, C.F. Martín, J.J. Pis, F. Rubiera, C. Pevida, Breakthrough adsorption study of a commercial activated carbon for pre-combustion CO2 capture, Chem. Eng. J. 171 (2) (2011) 549–556, https://doi.org/10.1016/j.cej.2011.04.027.
[75] M. Auta, U. Musa, M. Yahya, O. Adeniyi, M. Aris, B. Suleiman, Diethanolamine Functionalized Waste Tea Activated Carbon for CO2 Adsorption, 2015.
[76] M.K.A. Mesfer, M. Danish, M.I. Khan, I.H. Ali, M. Hasan, A.E. Jery, Continuous fixed bed CO2 adsorption: breakthrough, column efficiency, mass transfer zone, Processes 8 (10) (2020), https://doi.org/10.3390/pr8101233. Art. no. 10.
[77] H. Ramezanipour Penchah, A. Ghaemi, F. Jafari, Piperazine-modified activated carbon as a novel adsorbent for CO2 capture: modeling and characterization,

Environ. Sci. Pollut. Res. 29 (4) (Jan. 2022) 5134–5143, https://doi.org/10.1007/s11356-021-16040-5.
[78] M. Suba, O. Verdeş, S. Borcănescu, A. Popa, Effect of temperature on CO2 adsorption onto amine-functionalized KIT-6 adsorbents, Molecules 29 (13) (2024), https://doi.org/10.3390/molecules29133172.
[79] H.G. Ibrahim, M.A. Al-Meshragi, H.G. Ibrahim, M.A. Al-Meshragi, Experimental Study of Adsorption on Activated Carbon for CO_2 Capture, in: CO2 Sequestration, IntechOpen, 2019, https://doi.org/10.5772/intechopen.85834.
[80] Y.S. Ho, G. McKay, Pseudo-second order model for sorption processes, Process Biochem. 34 (5) (1999) 451–465, https://doi.org/10.1016/S0032-9592(98)00112-5.
[81] Y. Liu, X. Yu, Carbon dioxide adsorption properties and adsorption/desorption kinetics of amine-functionalized KIT-6, Appl. Energy 211 (2018) 1080–1088, https://doi.org/10.1016/j.apenergy.2017.12.016.
[82] C. Duan, T. Ma, J. Wang, Y. Zhou, Removal of heavy metals from aqueous solution using carbon-based adsorbents: a review, J Water Process Eng 37 (2020) 101339, https://doi.org/10.1016/j.jwpe.2020.101339.
[83] T.K. Saha, N.C. Bhoumik, Adsorption of Methyl Orange onto Chitosan from Aqueous Solution, ResearchGate, 2025 [Online]. Available: https://www.researchgate.net/publication/254862067_Adsorption_of_Methyl_Orange_onto_Chitosan_from_Aqueous_Solution.
[84] H. Jedli, M. Almonnef, R. Rabhi, M. Mbarek, J. Abdessalem, K. Slimi, Activated carbon as an adsorbent for CO $_2$ capture: adsorption, kinetics, and RSM modeling, ACS Omega 9 (2) (2024) 2080–2087, https://doi.org/10.1021/acsomega.3c02476.
[85] R. Ganjoo, S. Sharma, A. Kumar, M.M.A. Daouda, Activated carbon: Fundamentals, Classification, and Properties, 2025 [Online]. Available: https://books.rsc.org/books/edited-volume/2104/chapter/7568125/Activated-Carbon-Fundamentals-Classification-and.
[86] A.A. Tourzani, F. Hormozi, M. Asadollahzadeh, R. Torkaman, Effective CO2 capture by using poly (acrylonitrile) nanofibers based on the radiation grafting procedure in fixed-bed adsorption column, Sci. Rep. 13 (1) (2023) 6173, https://doi.org/10.1038/s41598-023-33036-y.
[87] E. Pancione, F. La Motta, A. Boffa, A. Lancia, A. Erto, Uncovering the Potential of Msc Ct-350 for Co2/Ch4 Separation Towards the Optimization of a Pressure Swing Adsorption Process for Biogas Upgrading, Social Science Research Network, Rochester, NY, 2023, https://doi.org/10.2139/ssrn.4672728, 4672728.